

A paper-based chemical tongue based on the charge transfer complex of

Sensor number	Name of the sensor	Contribution of each sensor on PCs with an array of metal-doped carbon dots	Sum of 3 PCs discriminates	Order of importance of sensors
---------------	--------------------	---	----------------------------	--------------------------------

natural amino acids and several of their enantiomers

Motahareh Alimohammadi ^a, Hoda Sharifi ^a, Javad Tashkhourian ^{a*}, M. Shamsipur ^b,

Bahram Hemmateenejad ^{a,c*}

^a *Chemistry Department, Shiraz University, Shiraz, 71454, Iran*

^b *Department of Chemistry, Razi University Kermanshah, Iran*

^c *Medicinal and Natural Products Chemistry Research Center, Shiraz University of Medical Sciences, Shiraz, Iran*

Corresponding Author

Chemistry Department, Shiraz University, Shiraz, 71454, Iran

*E-mail: hemmatb@shirazu.ac.ir, tashkhourian@shirazu.ac.ir

		PC1	PC2	PC3		
S1	Cr ³⁺ /CDs + Nin	0.075527	0.033305	0.072759371	0.1815908	8
S2	Mn ²⁺ /CDs + Nin	0.047133	0.141197	0.067672738	0.2560025	7
S3	Fe ³⁺ /CDs + Nin	0.143528	0.243312	0.19703618	0.5838768	1
S4	Co ²⁺ /CDs + Nin	0.037776	0.2374	0.095057272	0.3702324	3
S5	Ni ²⁺ /CDs + Nin	0.048417	0.068177	0.054568899	0.1711624	9
S6	Cu ²⁺ /CDs + Nin	0.166389	0.030243	0.134144315	0.3307761	5
S7	Zn ²⁺ /CDs + Nin	0.088181	0.097991	0.091143798	0.2773164	6
S8	Nin	0.241086	0.088612	0.136779248	0.4664771	2
S9	CDs + Nin	0.151964	0.059764	0.150838177	0.3625655	4

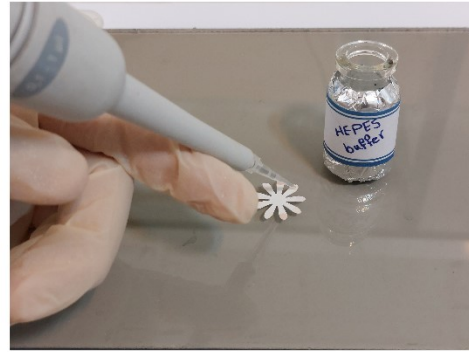
Table S1. Contribution abstained for each sensor on PCs using the variable selection method.

Table S2. The effect of the presence of sensors in order of importance in discrimination on accuracy of PCA-DA model.

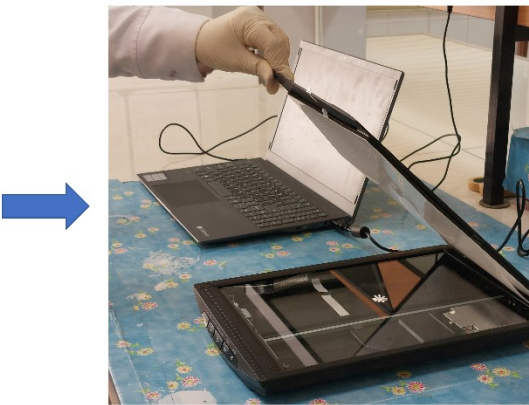
Sensor number	Accuracy (%)	
	Training	Cross-validation
S3	73	53
S3 and S8	98	88
S3, S8, and S4	100	93
S3, S8, S4, and S9	100	88
S3, S8, S4, S9, and S6	100	90
S3, S8, S4, S9, S6, and S7	100	97
S3, S8, S4, S9, S6, S7, and S2	100	98
S3, S8, S4, S9, S6, S7, S2, and S1	100	100
S3, S8, S4, S9, S6, S7, S2, S1, and S5	100	100



Injection of the sensing elements on the paper petals



Injection of HEPES buffer on the sensing elements in the petals



Scanning the PAD containing the sensing elements on the paper petal



Injection of amino acid solution in the central zone and then scanning the PAD

Figure S1. The actual pictures related to the process of this study.

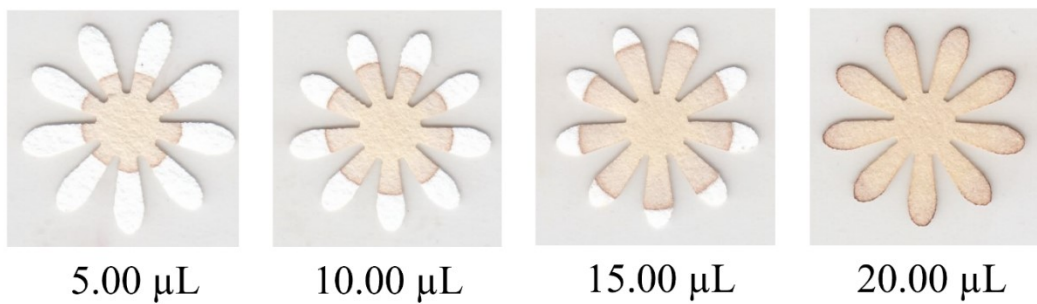


Figure S2. The appropriate amount of analyte covers all over the PAD.

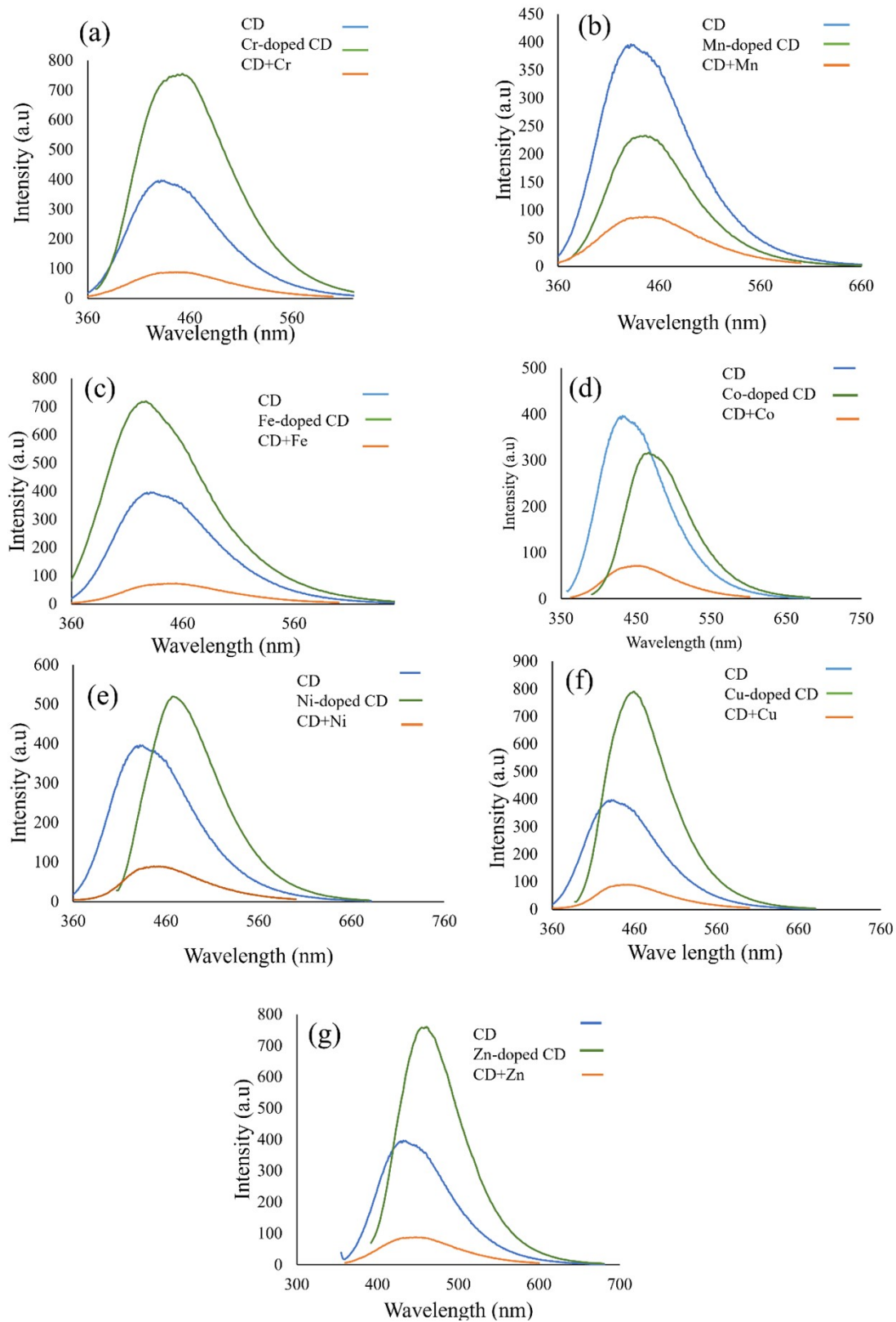


Figure S3. PL spectra of carbon dot (CD), metal doped carbon dots, and carbon dots in the presence of metal ions

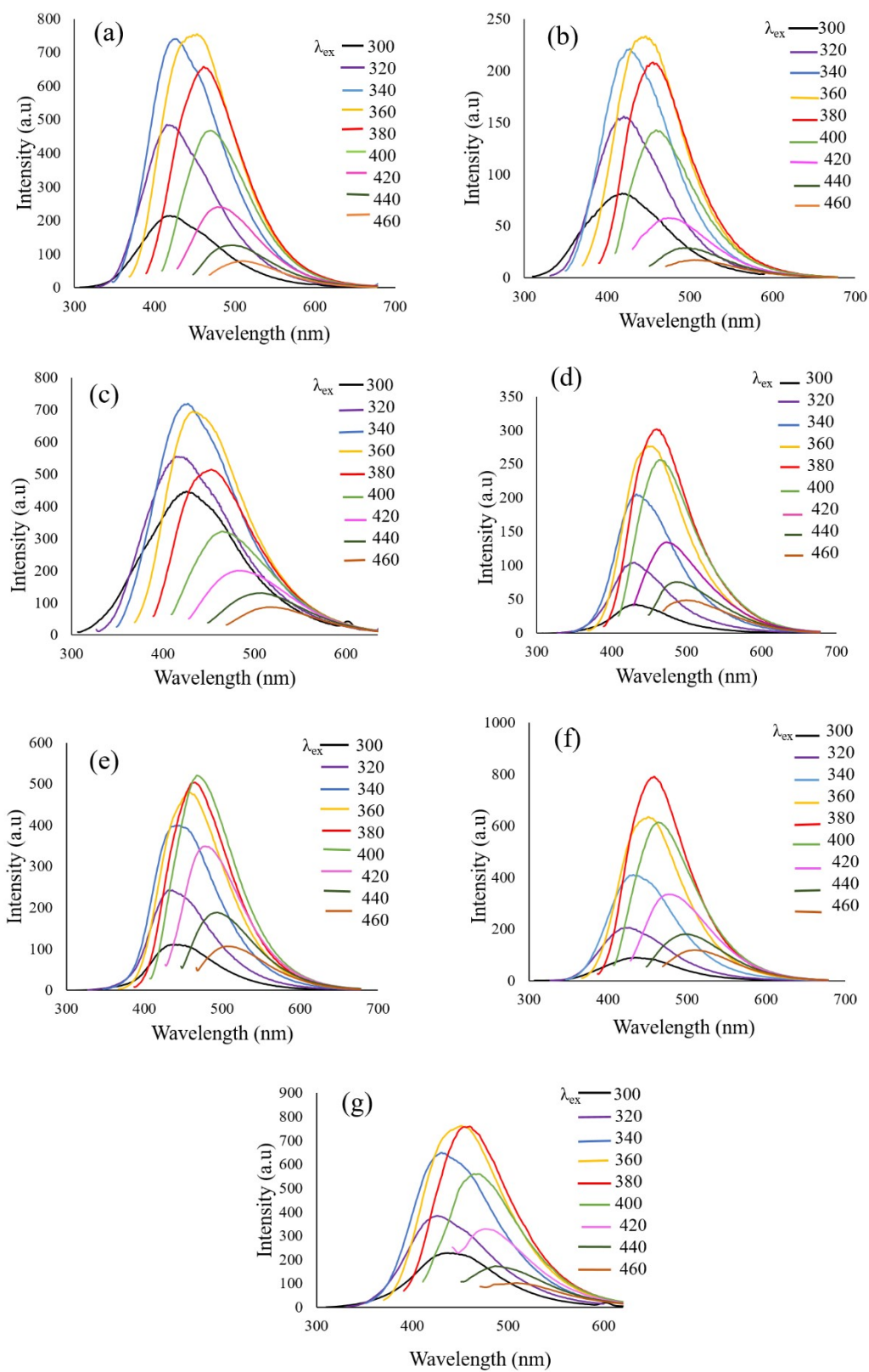
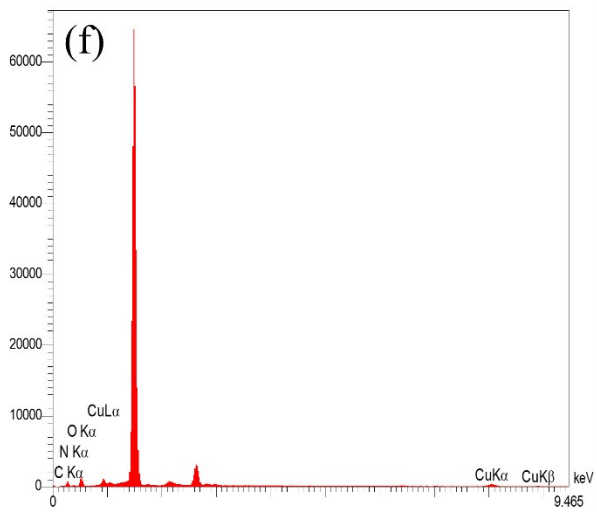
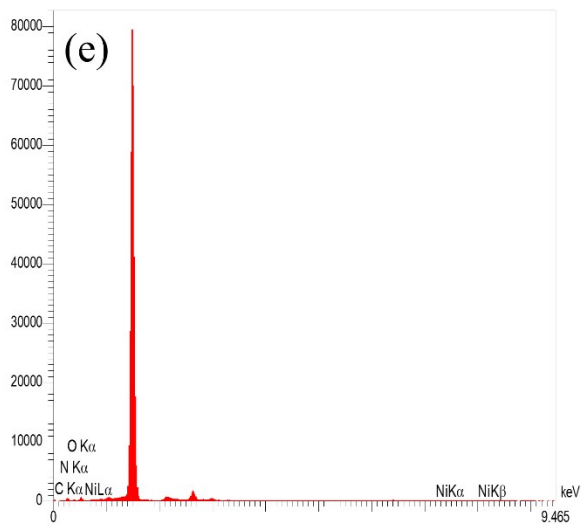
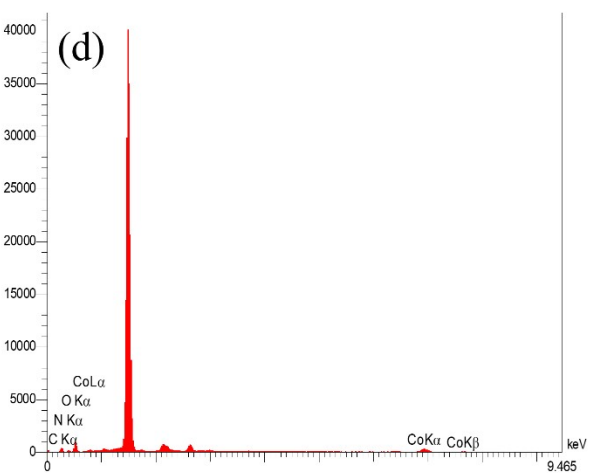
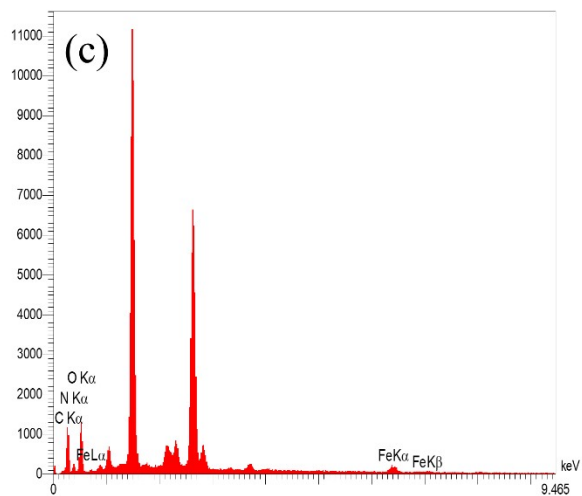
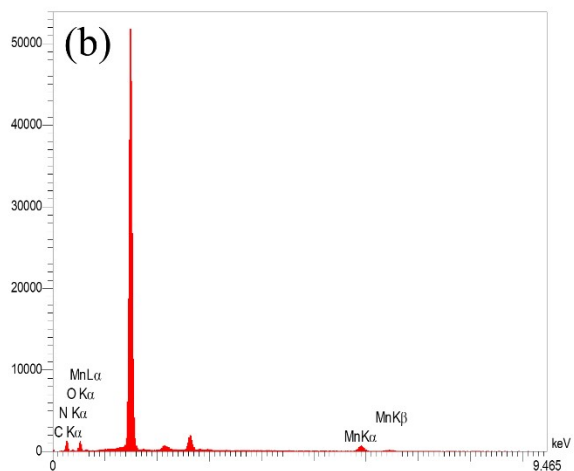
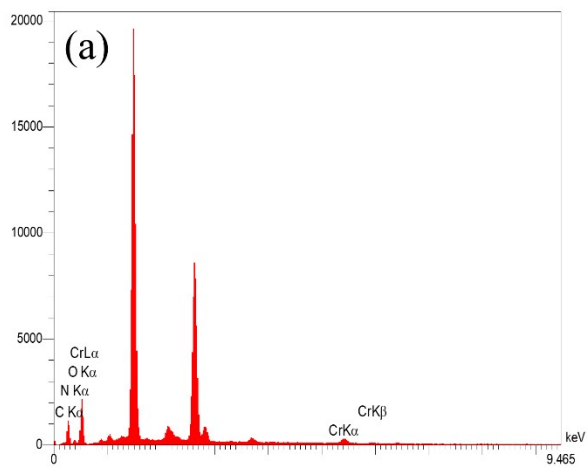


Figure S4. PL emission spectra of metal-doped CD with different excitation wavelengths (a-g (Cr^{3+}/C , Mn^{2+}/C , Fe^{3+}/C , Co^{2+}/C , Ni^{2+}/C , Cu^{2+}/C , and Zn^{2+}/C dots))



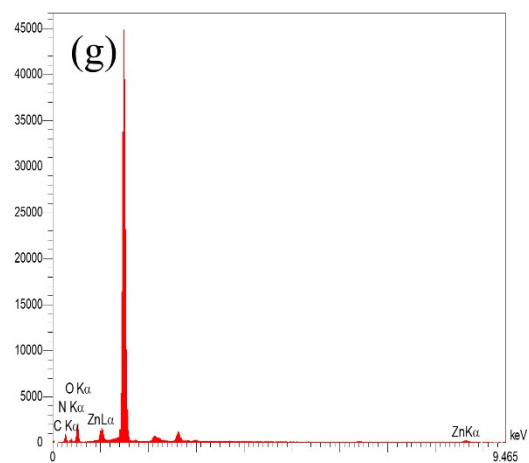


Figure S5. EDX analysis of metal-doped CDs (a-g (Cr³⁺/C, Mn²⁺/C, Fe³⁺/C, Co²⁺/C, Ni²⁺/C, Cu²⁺/C, and Zn²⁺/C dots)).

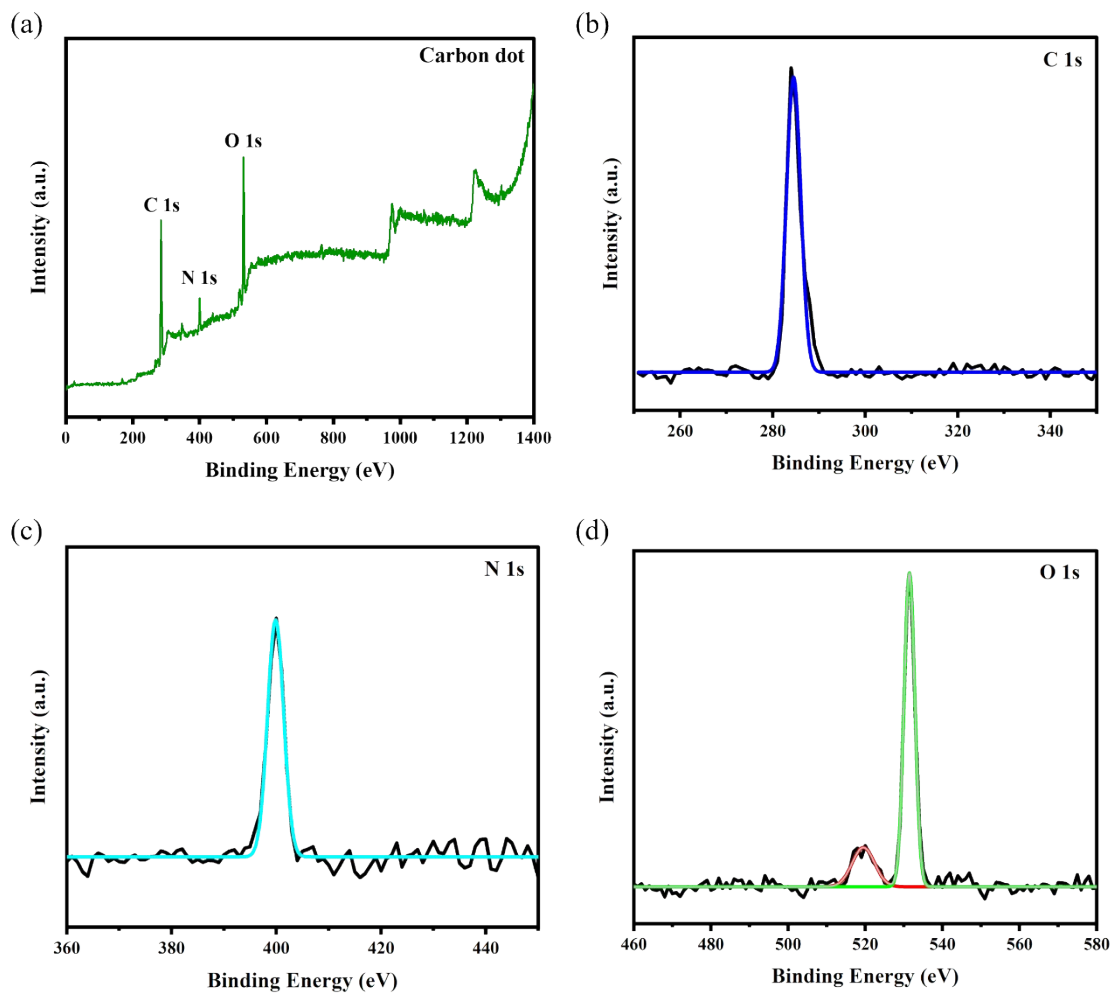


Figure S6. XPS survey spectrum of (a) CDs; High resolution spectra of (b) C 1s; (c) N 1s; (d) O 1s.

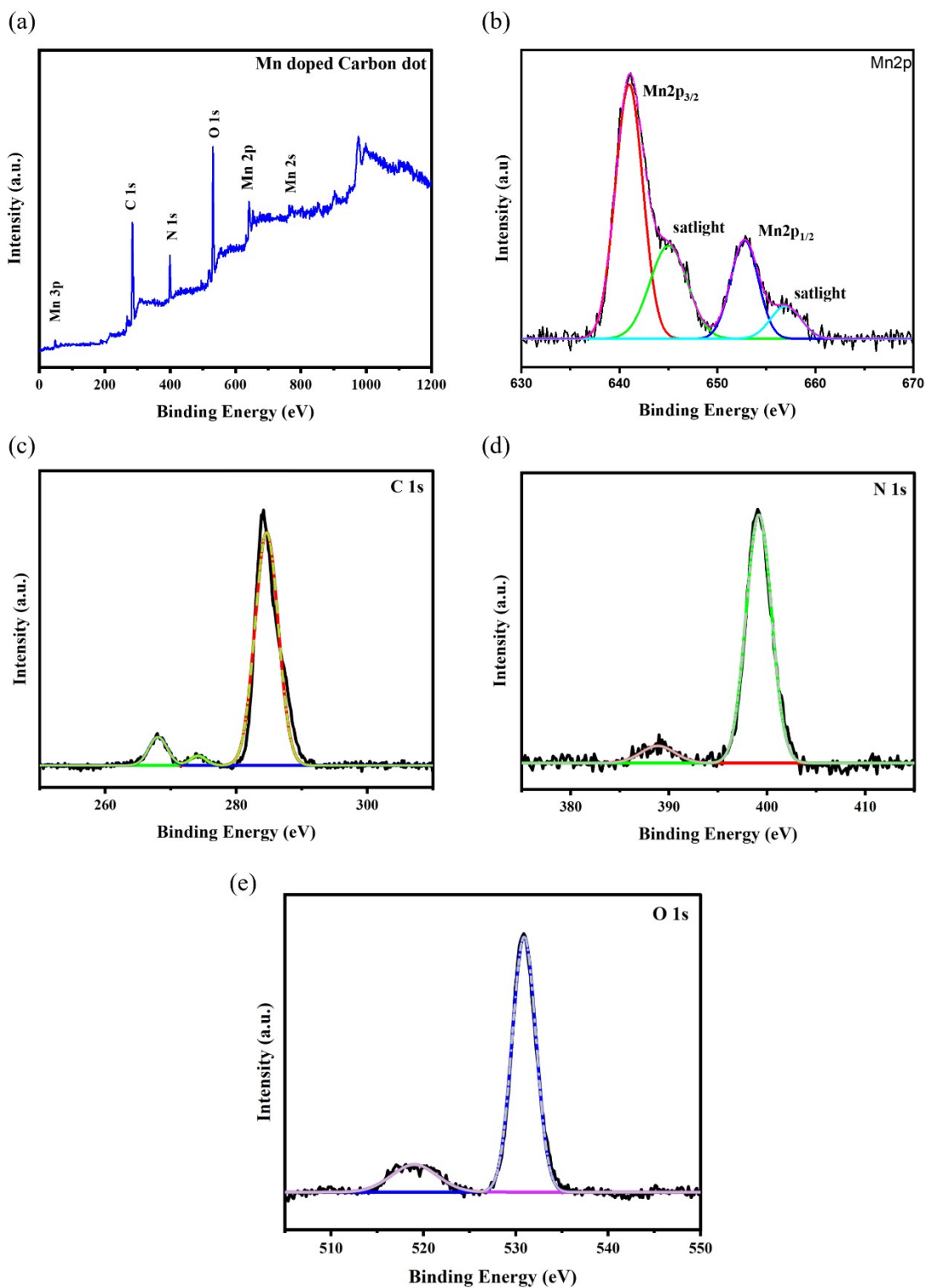


Figure S7. XPS survey spectrum of (a) Mn/CDs; High resolution spectra of (b) Mn 2p; (c) C 1s; (d) N 1s; (e) O 1s.

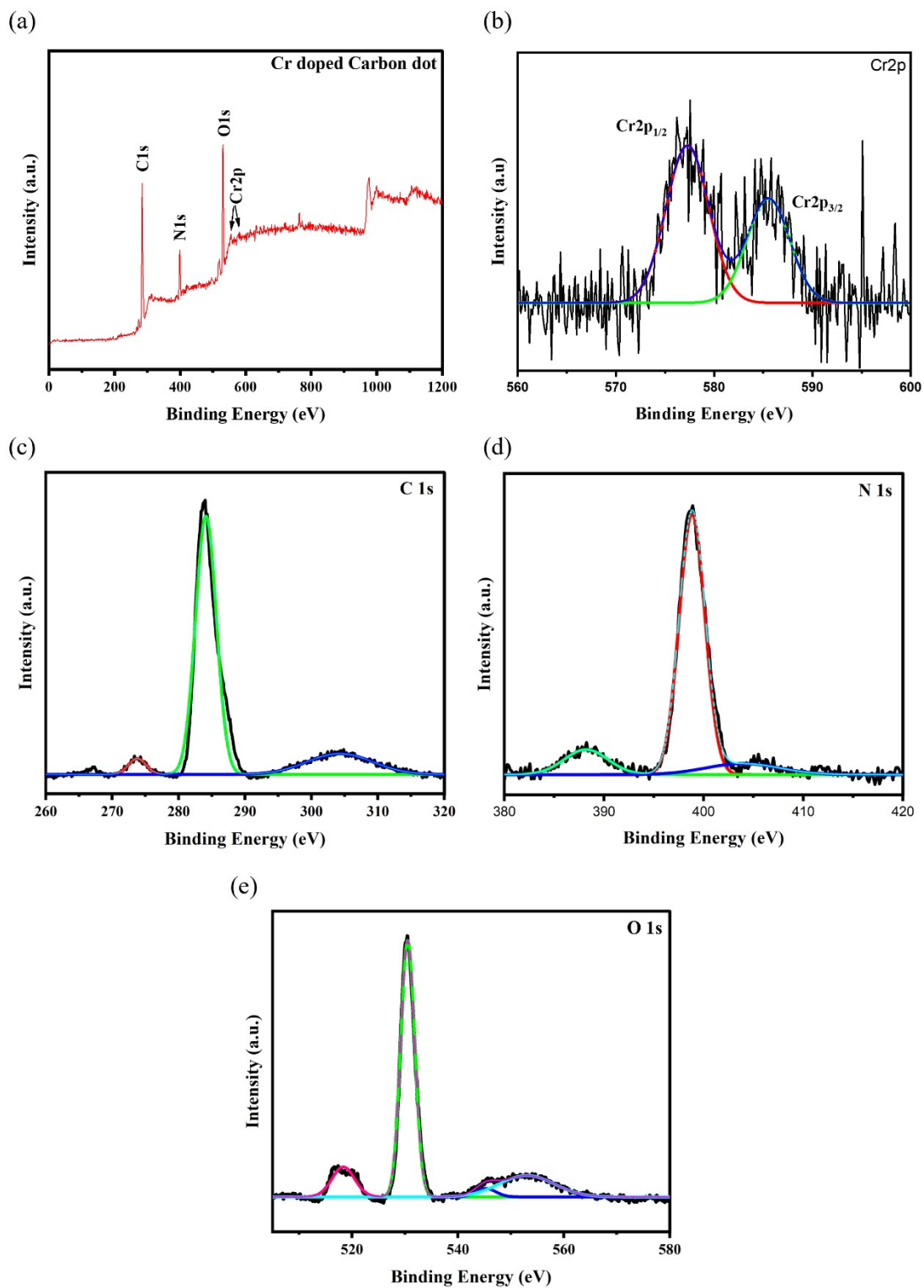


Figure S8. XPS survey spectrum of (a) Cr/CDs; High resolution spectra of (b) Cr 2p; (c) C 1s; (d) N 1s; (e) O 1s.

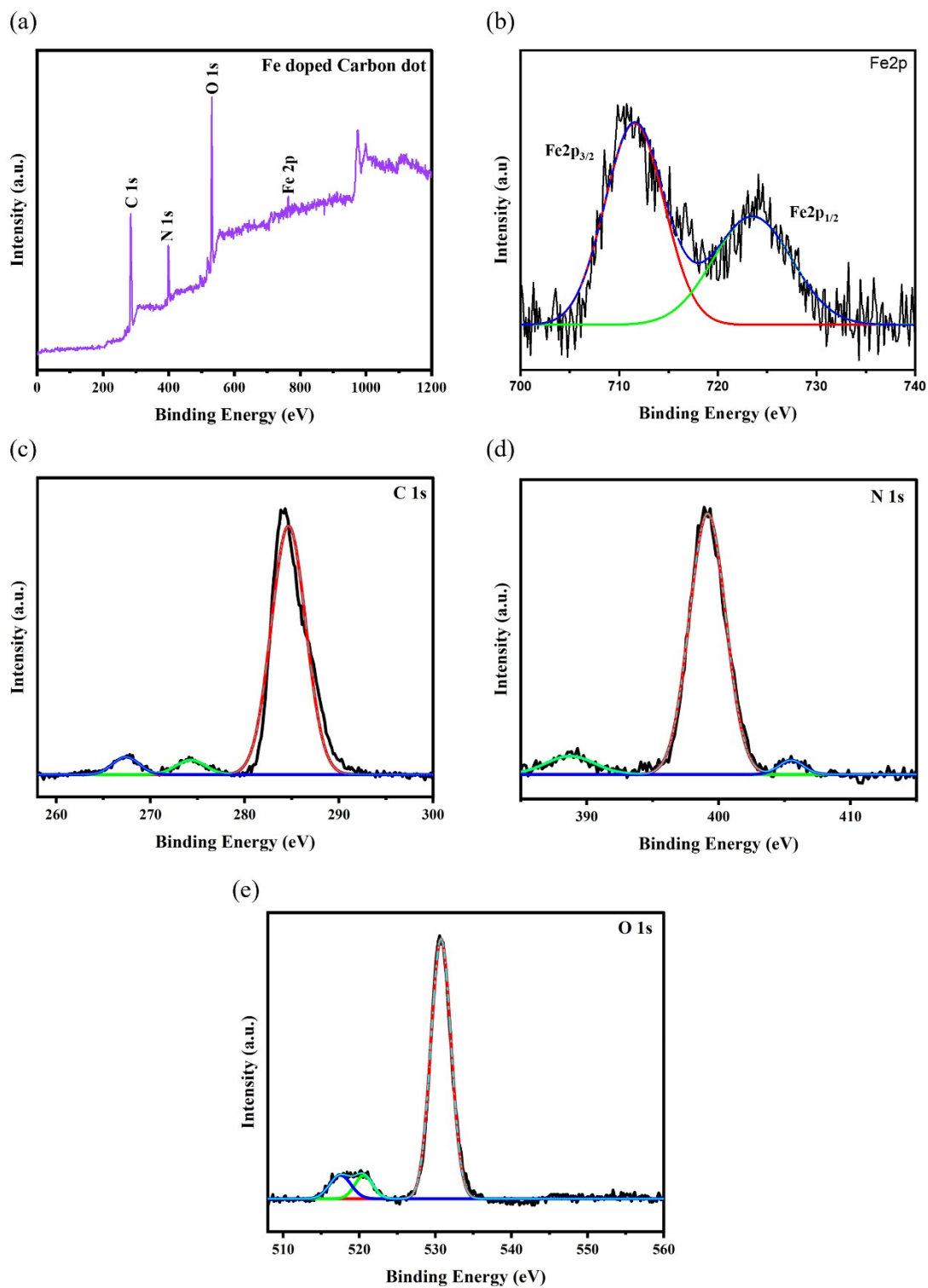


Figure S9. XPS survey spectrum of (a) Fe/CDs; High resolution spectra of (b) Fe 2p; (c) C 1s; (d) N 1s; (e) O 1s.

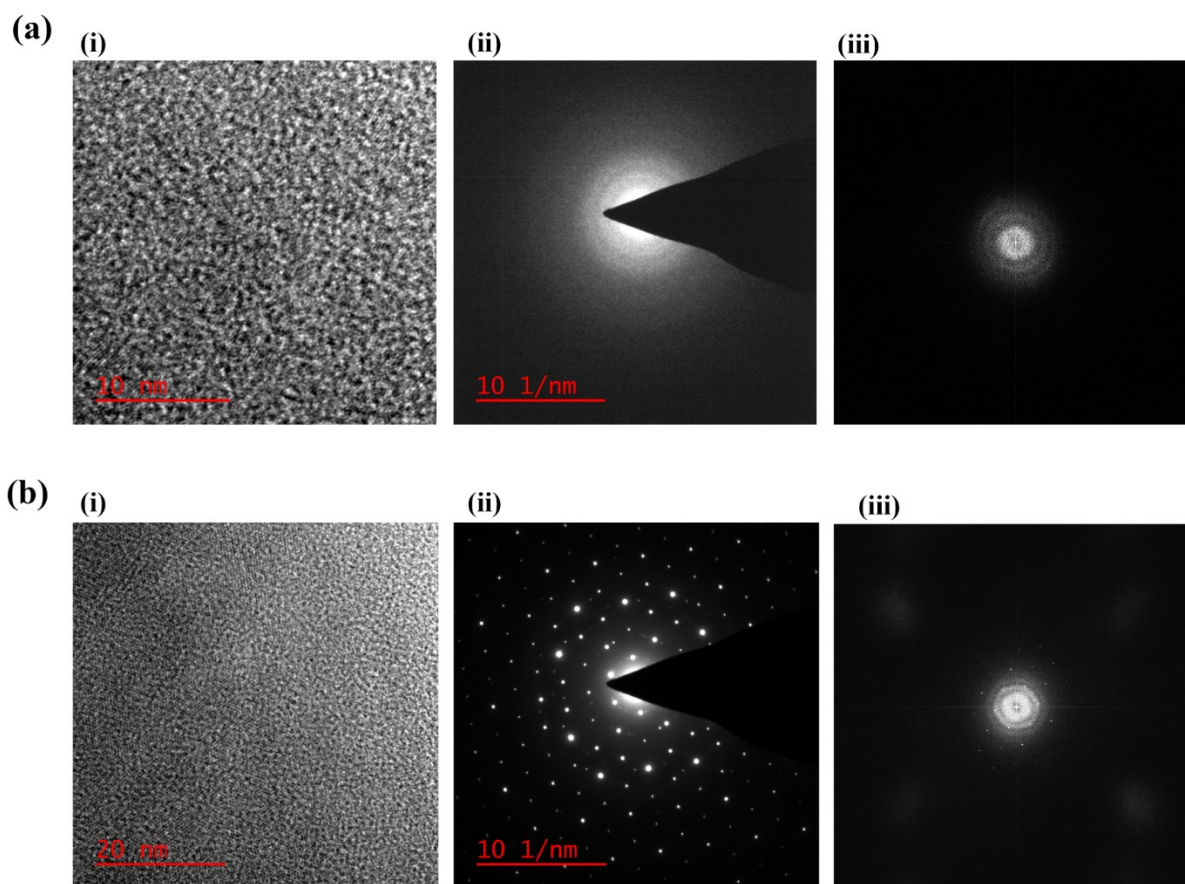


Figure S10. HRTEM images (i), selected area electron diffraction (SAED) (ii), and fast Fourier transform (FFT) (iii) patterns of (a) CDs and (b) Mn/CDs.

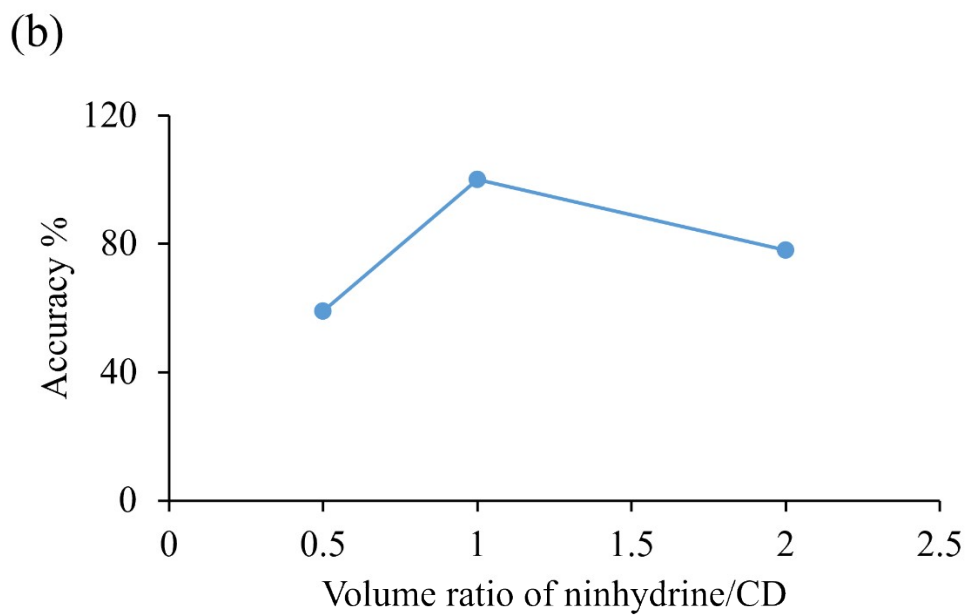
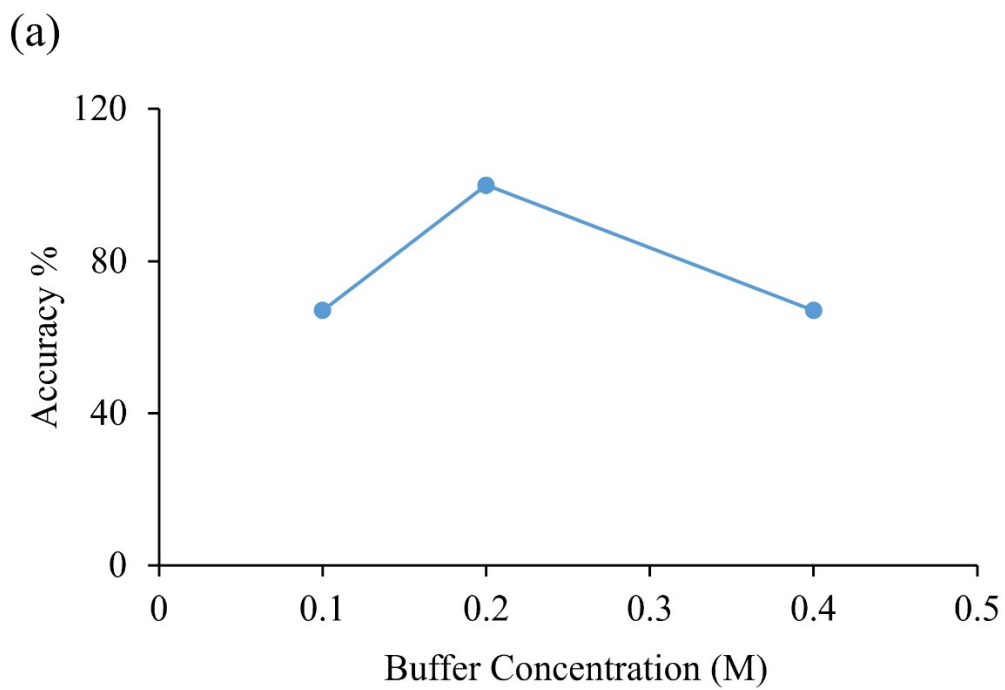


Figure S11. Effect of (a) HEPES buffer concentration (0.1 M, 0.2 M, and 0.4 M) and (b) volume ratio of ninhydrin/sensing elements (1:2, 1:1, and 2:1) on accuracy.

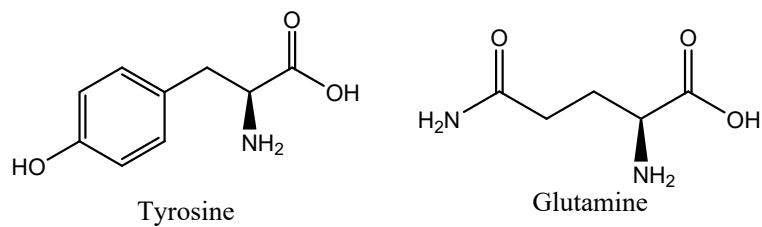
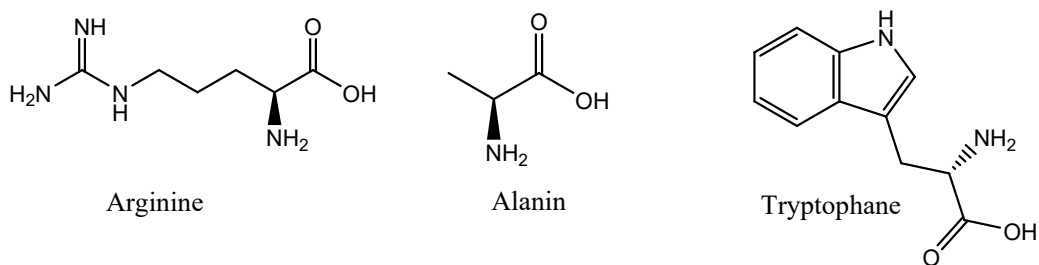
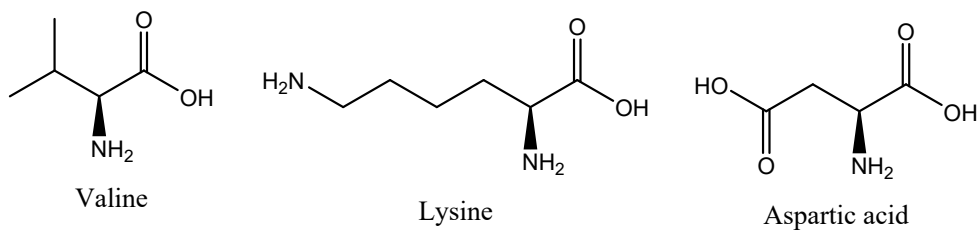
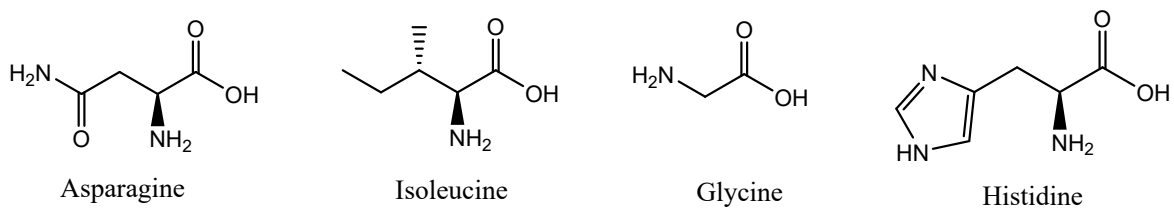
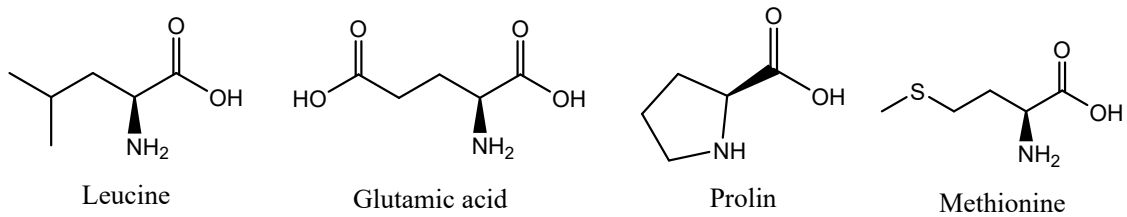
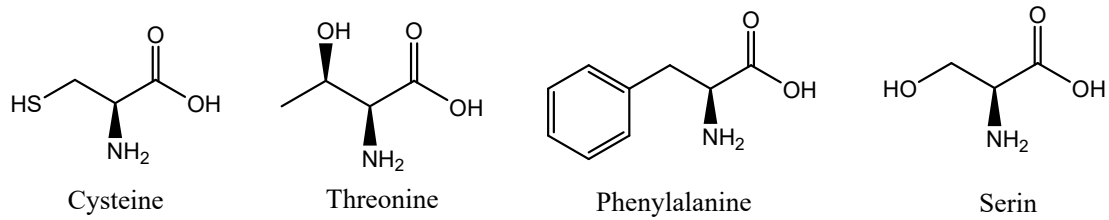


Figure S12. The molecular structures of used amino acids.

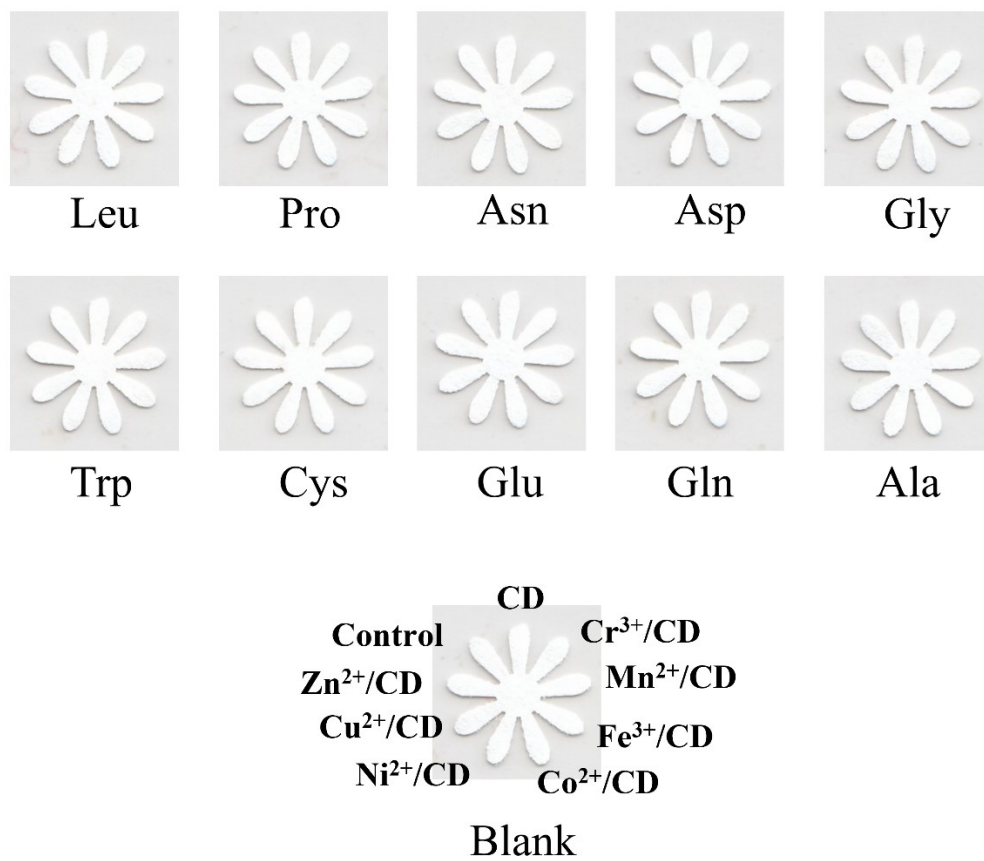


Figure S13. The reaction of PAD containing TMCDs in the absence of Nin against AAs.

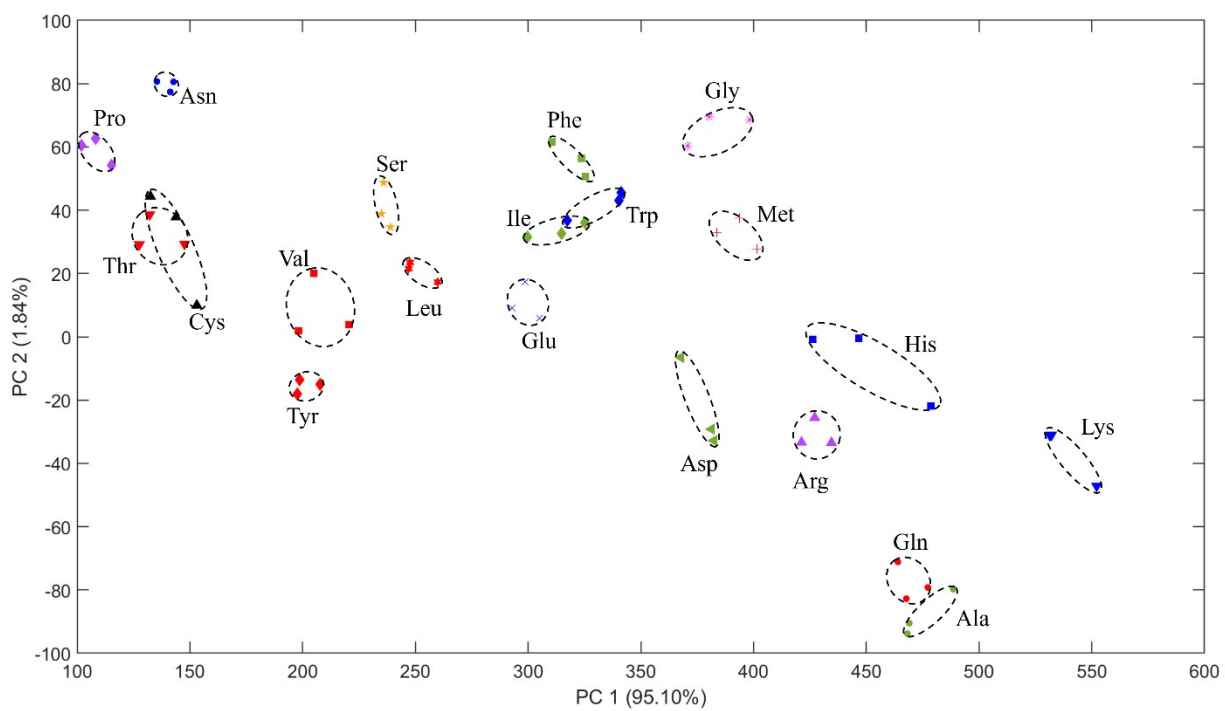


Figure S14. 2D PCA analysis for 20 AAs at a concentration of 10.00 mM. Ellipses indicate 95% confidence.

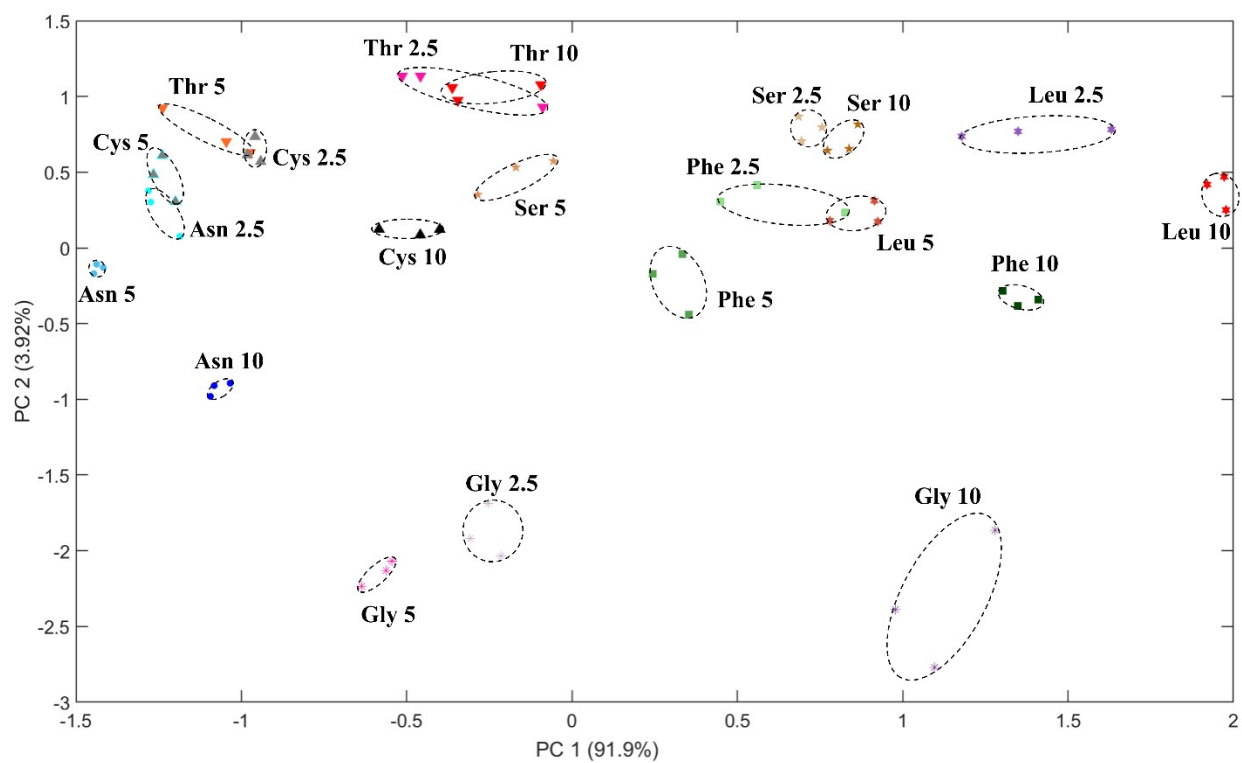


Figure S15. 2D PCA score plots for 7 amino acids: Cys, Leu, Thr, Asn, Ser, Phe, and Gly at three different concentrations (2.5, 5.0, and 10.0 mM) with an accuracy of 100%. Ellipses indicate 95% confidence.

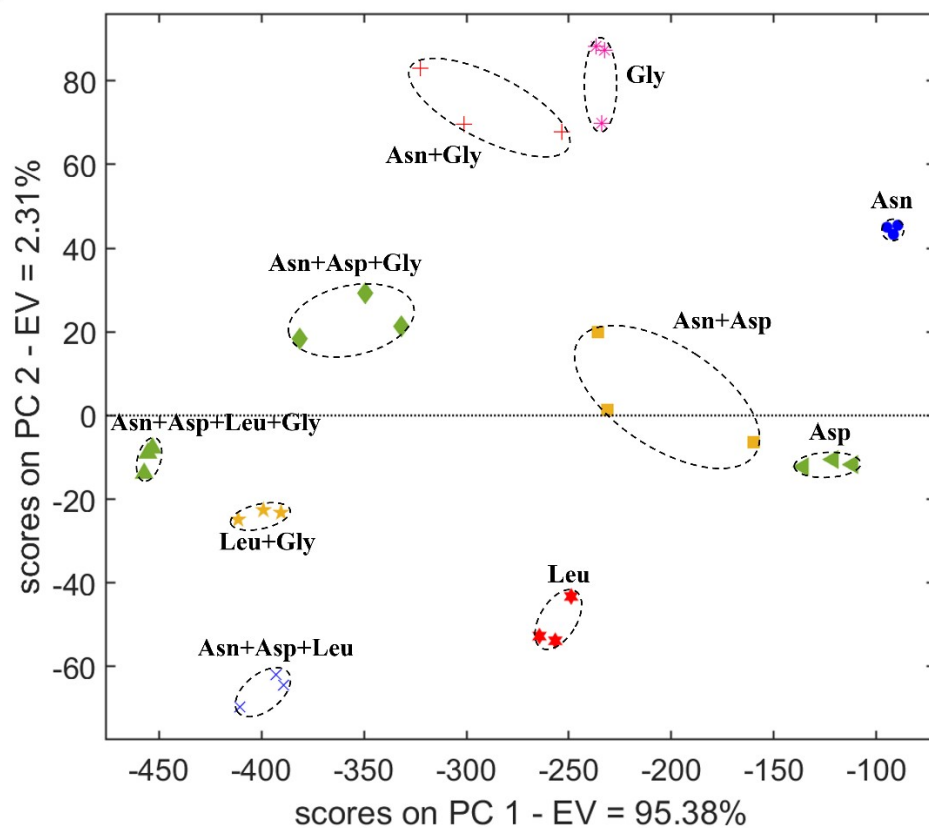


Figure S16. 2D PCA-DA plots for the binary, ternary, and quaternary mixtures of four different AAs (Leu, Asn, Asp, and Gly) with an accuracy of 100%. The total AAs concentration was 10.0 mM. Ellipses indicate 95% confidence.

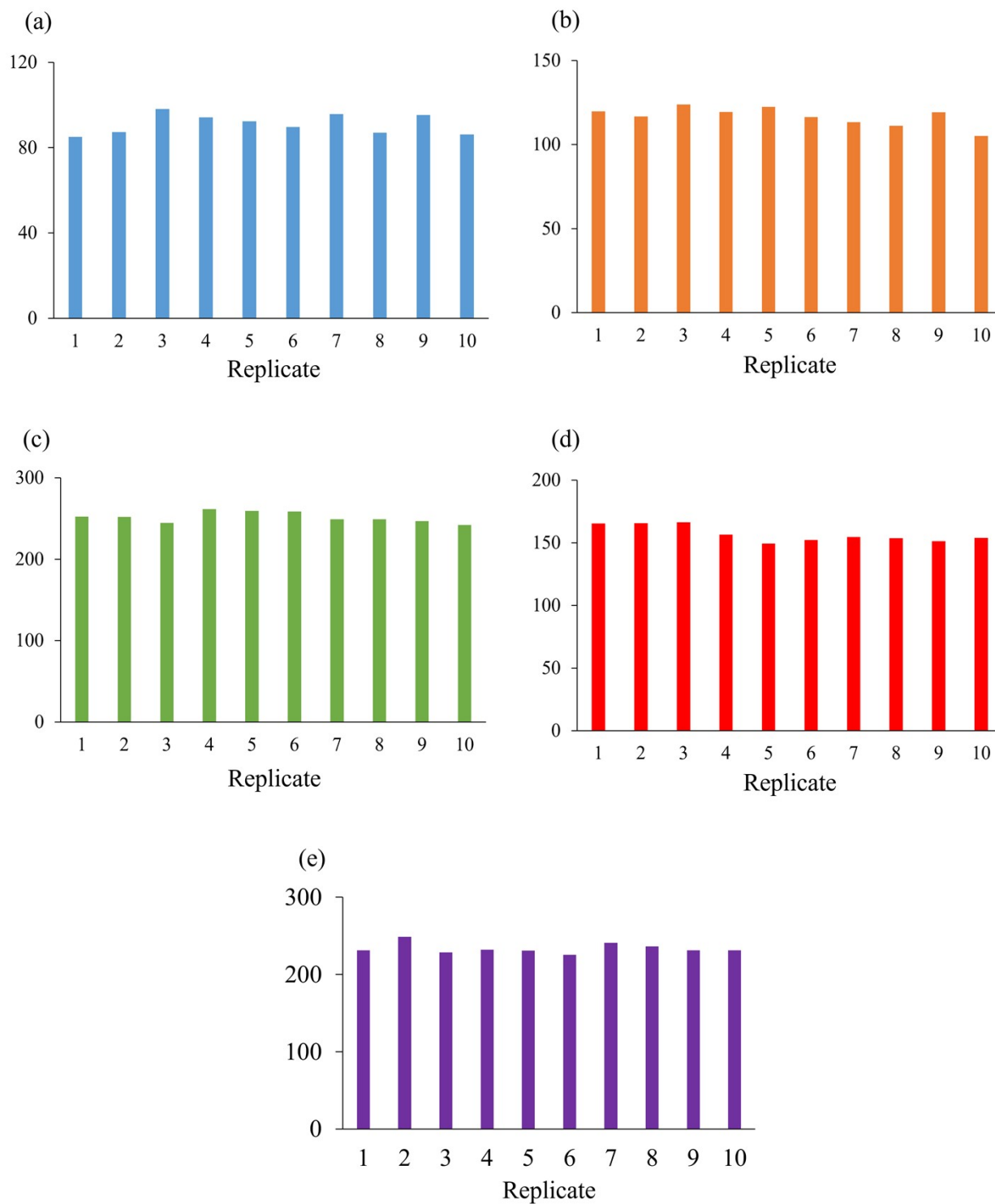


Figure S17. The reproducibility of the response of sensor array for detection of 10.0 mM of 5 amino acids (a) Cys, (b) Asn, (c) Met, (d) Trp, and (e) Phe. The Euclidean distance is the total length of the full dimensional color-difference vector, that is, the total array response.

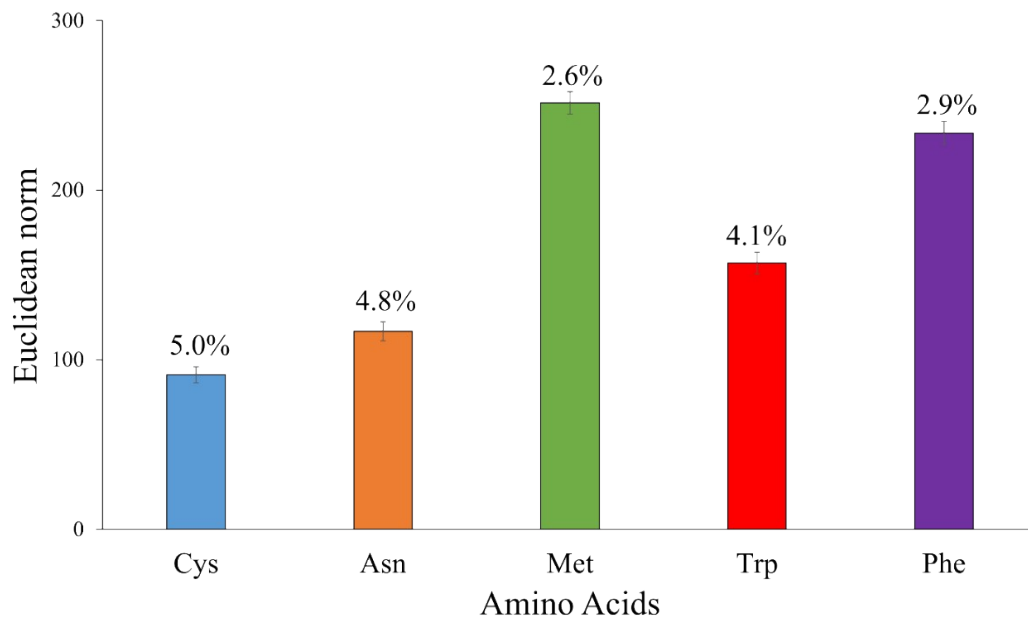


Figure S18. The coefficient of variations of the response of the sensor array for five amino acids in ten replicate measurements. The error bars show the standard deviation of ten independent measurements. Relative standard deviations were displayed on the top of the bars.

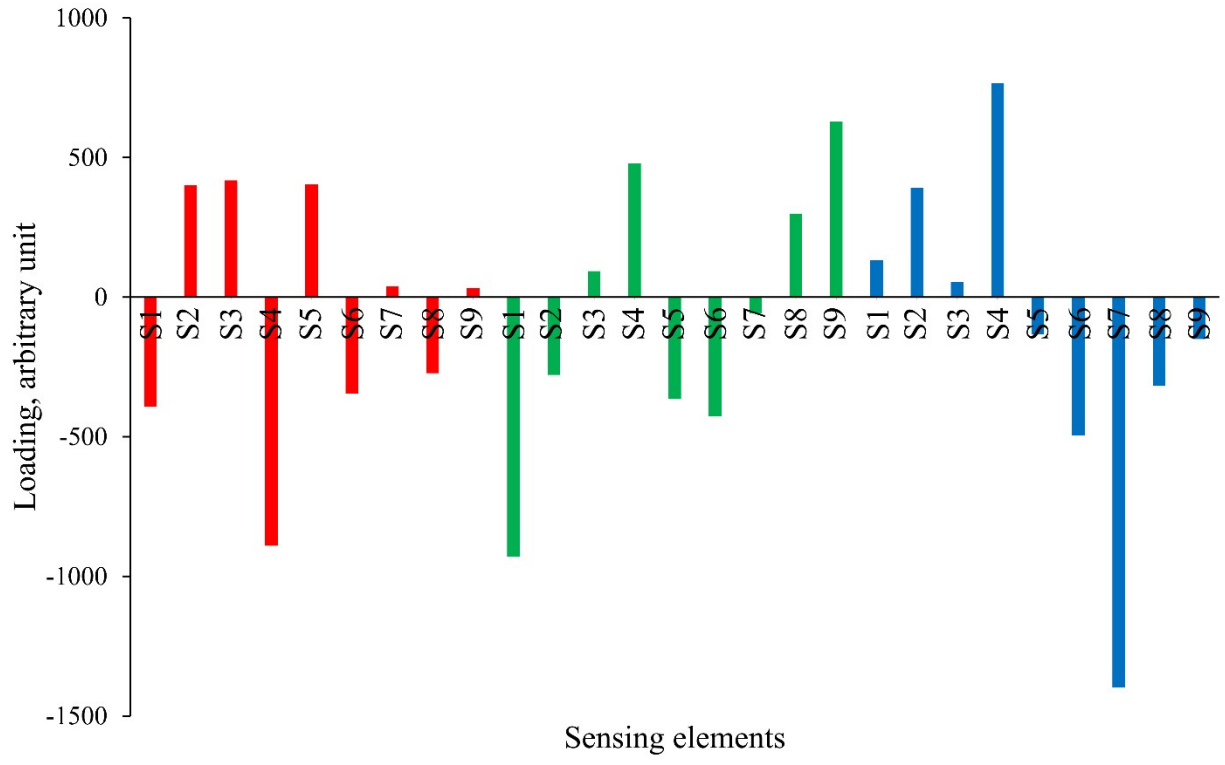


Figure S19. Plot of the first PCA factor loadings. S1, S2, S3 S4, S5, S6, S7, S8, and S9 represent metal-doped CDs (Cr^{3+}/C , Mn^{2+}/C , Fe^{3+}/C , Co^{2+}/C , Ni^{2+}/C , Cu^{2+}/C , and Zn^{2+}/C dots), respectively.